Experimental Investigations of Fluid Dynamics of Gravity-destabilized Liquid Film Flows over Structured Surfaces Using Light Induced Fluorescence

Hannes Raddant[a], Georg Brösigke[a], Christian Hoffmann[a], Markus Illner[a], Jens-Uwe Repke[a]

[a] Technische Universität Berlin, Process Dynamics and Operations Group, Str. des 17. Juni 135, 10623 Berlin, Germany
raddant@tu-berlin.de; georg.broesigke@tu-berlin.de; c.hoffmann@tu-berlin.de; markus.illner@tu-berlin.de; j.repke@tu-berlin.de

Abstract. While film flows are widely investigated, specifically gravity-destabilized film flows have not been studied thoroughly so far. Thus, this contribution, investigates the influence of structured surfaces on the fluid dynamics of gravity-destabilized liquid film flows by means of Light Induced Fluorescence (LIF). Results on critical inclination angle, mass flow of the drained liquid, and liquid film thickness without gas counterflow are presented and compared to literature data. The experiments were conducted in an aqueous system whose surface tension was adjusted with the help of an additive. The experimental Reynolds number varied from 25 to 100. A flat plate, 2D wave, and 3D pyramid structure, which is typically used in structured packings, were investigated. Under these experimental conditions, a negative influence of the 2D structure on the liquid flow stability due to intensification of present Rayleigh-Taylor instabilities was found. In contrast, the 3D structure seemed to stabilize the liquid flow.

Keywords Fluid dynamics, Liquid film flow, Structured surface, Rayleigh-Taylor instability

Introduction

In distillation and absorption processes, structured packings are used to improve mass transfer and fluid dynamic performance. The flow regime inside the packing material depends on operating parameters, fluid properties, and column/packing design. Under normal operating conditions, the liquid flows down the structured packing material as a liquid film or as rivulets. Therefore, two liquid flow conditions may be present. The gravity-stabilized and the gravity-destabilized liquid film flow. The main difference between both liquid film flow conditions is the direction of gravity [13]. For the gravity-destabilized liquid film flow, the liquid phase with higher density flows above the gas phase with lower density. This density difference results in the occurrence of Rayleigh-Taylor instabilities due to the phase arrangement. Unlike gravity-stabilized liquid film flows, for which profound knowledge of fluid dynamics on both flat and structured surfaces has been gained experimentally and numerically [6,8,9,10,11,12], knowledge of the fluid dynamics of gravity-destabilized liquid film flows is very limited [2,3,4]. However, gravity-destabilized liquid film flow likely accounts for half of the flow in packing materials and hence should be understood in detail to enable optimization of packing design. In detail, the separation performance of structured packing columns could be influenced by droplet detachment and liquid film thickness. Therefore, increased back mixing caused by droplet entrainment of detached liquid may reduce the overall separation efficiency. The back-mixing effect and the liquid film thickness may reduce the free gas flow area, and result in a higher pressure drop across the column. For absorption processes, droplet detachment could increase liquid mixing inside the packing channels. This effect results in a higher penetration depth and may increase gas-liquid mass transfer. Hence, understanding the fluid dynamic behavior of gravity-destabilized liquid film flows in structured packings is necessary to further understand the overall fluid dynamic and mass transfer performance in distillation and absorption columns.

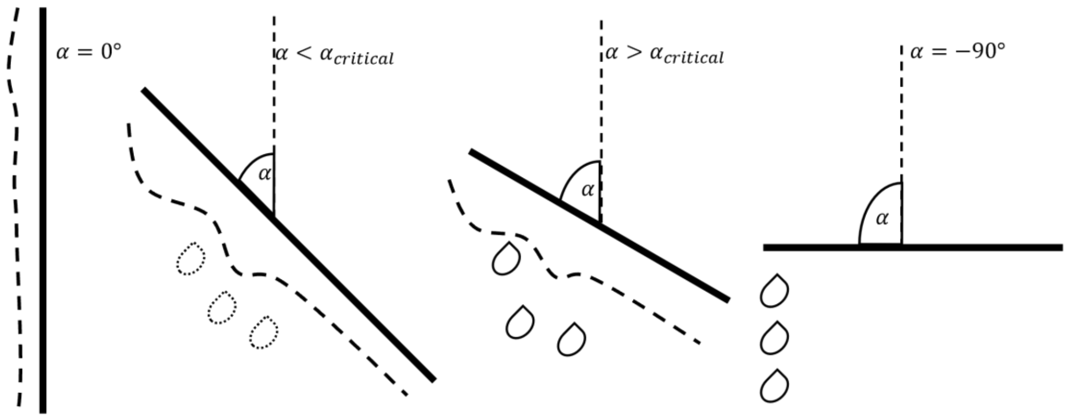

a) Vertical liquid fall film.
b) Negative inclined liquid fall film with convective Rayleigh-Taylor instability.
c) Negative inclined liquid fall film with predominantly absolute Rayleigh-Taylor instability.
d) Horizontal liquid fall film.

Fig. 1 Droplet detachment phenomena of falling liquid films at different inclinations and prevailing Rayleigh-Taylor instabilities.

Fig. 1 shows four different flow conditions for gravity-destabilized liquid film flows. For the vertical falling liquid film (case a), gravity accelerates the liquid flow the most and no Rayleigh-Taylor instabilities or droplet detachment occurs. Case b) occurs, when the negative inclination angle α is lower than the critical angle $\alpha_{critical}$ for the transition between convective and absolute instability [1]. The critical angle describes the transition from irregular convective liquid dripping to regular permanent droplet detachment induced by Rayleigh-Taylor instabilities. The liquid flow is less accelerated compared to case a) and convective instabilities could be present for this arrangement. Convective instabilities are induced due to the prevailing convective liquid flow and the current liquid flow regime e.g., rivulet flow or film flow. These form of instability results in irregular and not constant droplet detachment. Once the inclination angle α is larger than the critical angle, absolute Rayleigh-Taylor instability occur (case c). The state of absolute Rayleigh-Taylor instability is characterized by regular droplet detachment out of the closed liquid film flow. Under these conditions, the liquid drains out of the closed film flow depending on the Reynolds number $Re = \rho \cdot v \cdot d \cdot \eta^{-1}$, the Kapitza number $Ka = \sigma \cdot g^{-1/3} \cdot \upsilon^{-4/3} \cdot \rho_L^{-1}$, and the inclination angle α [5]. Finally, case d) describes a horizontal liquid flow, for which absolute Rayleigh-Taylor instability is fully developed and the liquid drains completely. For a laminar liquid film flow, the film thickness δ depends on the Reynolds number Re, the inclination angle α, and the kinematic viscosity ν and can be calculated using eq. (1) for Reynolds numbers smaller 400 [1,7].

$$\delta = \left(\frac{3 \cdot \upsilon_L^2}{g \cdot \cos \alpha} \right)^{1/3} \cdot Re^{1/3} \quad (1)$$

Likewise, α depends on the Reynolds number and the surface structure. To understand the gravity-destabilized flow regime, we investigate the critical inclination angle α, the relative detached liquid mass flow, and the mean film thickness δ for different Reynolds numbers and three different surface structures (flat, 2D, and 3D).

Materials and Methods

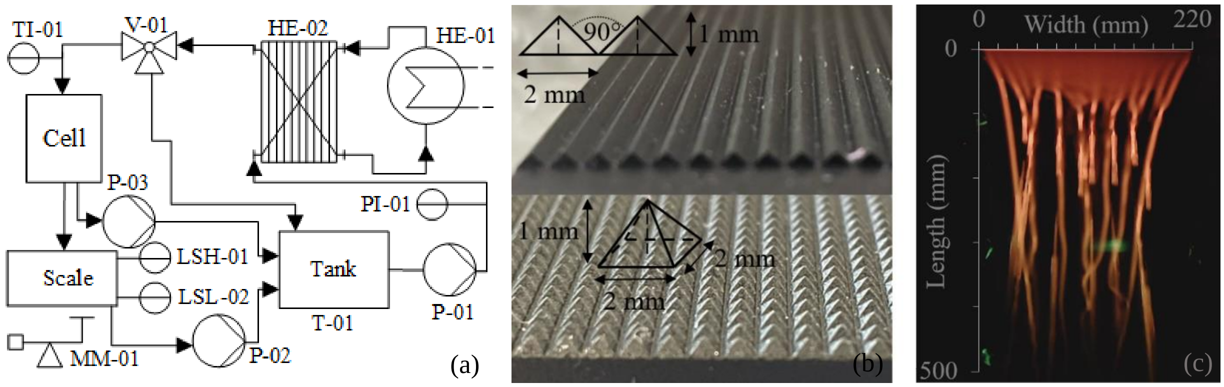

Fig. 2 Plant flowsheet (a), the investigated surfaces (b) and a LIF picture of a gravity-destabilized aqueous film flow (c).

The experimental setup consists of a liquid cycle, a rotatable measurement cell, a balance, and a camera setup (Fig. 2 a). A liquid distributor ensures that all pumped liquid is evenly distributed. The rotatable cell is attached to a planetary geared stepper motor, which is used to set any plate inclination. The theoretical parameterized precision is α ±0,01°. The optical setup contains a pco.2000 CCD-camera equipped with an optical lens and a red-light bandpass filter. As the fluorescence excitation light source two green LED bar light are used. These obtain a constant and reproducible excitation over the whole measuring time. A camera housing with a transparent optical glass window has been installed as splash protection. The liquid phase consists of water with adjusted surface tension (σ < 33 mN m^{-1}, Marlipal 24/70 (c ≥ cmc) from Sasol). The surface tension is watched using a tensiometer with the Wilhelmy plate method. Rhodamine B is added (concentration of around 5 mg L^{-1}) as a fluorescence tracer. The experiments were performed on anodized aluminum surfaces with a width of 220 mm and a length of 500 mm. The liquid temperature is set to 25°C ±0,1°. The flow rate is controlled, and the pressure is monitored. All experimental runs are initialized with conditions for a fully wetted surface at α = 0° (Fig. 1 case a). To measure the drained liquid mass flow, the cell is rotated to different negative α and a minimum measuring time of 180 s per experimental point is conducted. Afterwards $\alpha_{critical}$ is determined by evaluation of the first weighed liquid from mass signal over time signal. The mean film thickness is measured via LIF for a 10 cm x 10 cm region of interest in the middle of a surface structure (approx. 5 cm after the inlet). In the post processing, background correction is used to reduce the impact of reflections. Since the fluorescence signal is based on the excitation light intensity, illumination correction is applied to ensure the measured fluorescence signal to be decoupled from the local excitation light intensity. Moreover, an offset calibration and a temperature calibration is carried out for the calibration cuvette.

Results and Discussion

In the first step, the experimental results are compared to published numerical data for a flat plate by Scheid et. al. [1]. In Table 1, literature values for $\alpha_{critical}$ calculated with given correlation for imposed film thickness are shown. The critical inclination angle is measured for the aqueous system with a Kapitza number around 1457. Scheid et. al. predicted the occurrence of a minimal negative critical inclination angle for Re ≈ 8 and Ka = 1457. However, our experiments could only be carried out at Re ≥ 25. Otherwise, we could not achieve a fully wetted surface for the vertical falling film with α = 0°.

Table 1.
Critical inclination angle for flat plate at different Reynolds numbers for 25°C and comparison with literature data.

Reynolds number	25.25	31.57	37.88	75.76	101.01
Theoretical critical inclination angle $\alpha_{critical}$ [1]	−83.1°	−82.7°	−82.4°	−81.0°	−80.3°
This study exp. critical inclination angle $\alpha_{critical}$	−84.4°	−84.4°	−80.5°	−79.5°	−79.5°

The results in Table 1 indicate a good agreement between our experimental results and the correlation given by Scheid et al. [1] for the flat plate. Across all measured points, a deviation of under 2° could be observed. The slight deviation of the experimental results can be explained with non-ideally distributed liquid at the entry of the plate. The flat plate is technically flat, so the surface is not ideal smooth and can affect the liquid flow. In combination with the effect of rivulet confluence, which could be observed in the experiments, higher local film thickness and larger local Rayleigh-Taylor instabilities result in liquid drainage at lower negative α, except for Re from 25 to 32. Finally, the drainage of liquid occurs out of a three-dimensional domain. However, the simulation result from Scheid et al. is based on a two-dimensional model [1].

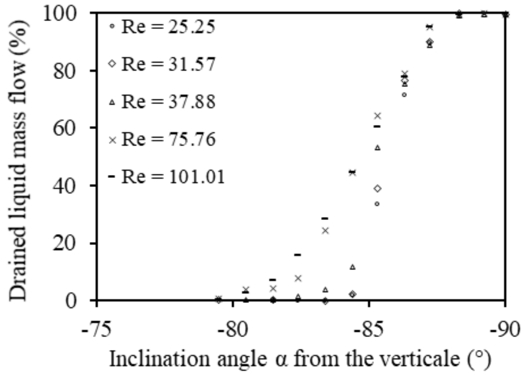

Fig. 3 Drained mass flow for surface tension adjusted aqueous system with Ka = 1457 at 25°C on flat surface.

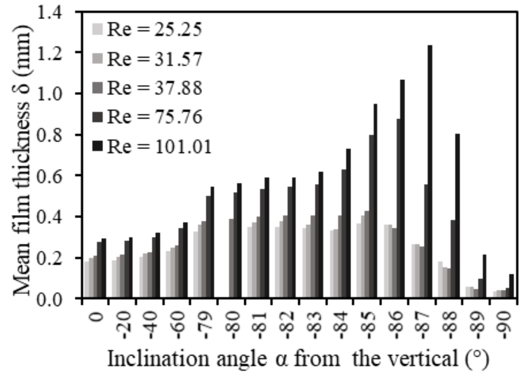

Fig. 4 Measured film thickness for surface tension adjusted water with Ka = 1457 at 25°C on flat surface (angles rounded).

In Fig. 3 the drained liquid mass flows depending on the Reynolds number and α is shown. With increasing Reynolds number, the relative drained liquid mass flow overall increases. Moreover, $\alpha_{critical}$ decreases with higher Reynolds numbers which indicates higher convection destabilization under these operation conditions. For increasing Reynolds number, the curve slope after the dripping onset gets smaller. However, a significant quantity of liquid drains at this operating conditions. Higher Reynolds numbers lead to higher relative drained mass flows for the same α, except for Re = 75.76 and for Re = 101.01 at α = −81.5°. This result is caused by rivulet confluence, which is a non-controllable operating condition. Deviations for α = −85.4° and α = −86.5°, from the observed general trends can be explained by the flow stabilization due to higher liquid velocity [1]. In Fig. 4, the experimental mean film thickness is shown for varying Reynolds numbers and different inclination angles. A comparison to the theoretical film thickness computed with Eq. (1) is demonstrated in Table 2.

Table 2.
Mean film thickness for a flat plate at different Reynolds numbers for 25°C and α = 0°.

Reynolds number	25.25	31.57	37.88	75.76	101.01
Theoretical film thickness δ calculated with Eq. 1	0.197 mm	0.213 mm	0.226 mm	0.285 mm	0.314 mm
This study exp. mean film thickness	0.181 mm	0.199 mm	0.211 mm	0.280 mm	0.294 mm

The mean film thickness increases with higher Re and is in the range of 0.181 to 0.294 mm for Re from 25 to 101 and α = 0°. The film thickness increases with higher Reynolds number for α ≤ −81°. This observation is expected based on literature data [8]. For α in the range from −79° to −84°, the film thickness increases less significantly for all investigated Reynolds numbers. For α from −85° to −88° droplet detachment occurs and hinders the observation of the image area, as the droplets distort the measurements by reflexions and overexposure. Therefore, the measured film thickness in this range of α show an increased measurement error. This effect is more significant for Re ≥ 75 due to larger drained liquid mass flow as shown in Fig. 3. For α from −85° to −88° droplet detachment is observed, and a decreased film thickness is expected. The decreased mean film thickness with increased inclination for Re from 25 to 38 numbers is physically sound. In contrast, the observed increase of the film thickness for Re from 75 to 100 with α ≥ $\alpha_{critical}$ contradicts mass conservation if a significant share of the liquid drains. For a critical inclination near the horizontal position (α ≤ −89°), distortion by droplets is no longer given and reasonable mean film thicknesses are calculated again. The measured values represent the mean film thickness, however, there is no longer a convective liquid flow along the flat plate.

Table 3.
Experimental $\alpha_{critical}$ for the flat plate, 2D wave structure and 3D pyramid structure at different Reynolds numbers for 25°C. Results for flat plate and 2D structure were repeated once, 3D results were measured once. The repetition is currently done.

Reynolds number	25.25	31.57	37.88	75.76	101.01
Exp. critical inclination angle α flat plate	−84.4°	−84.4°	−80.5°	−79.5°	−79.5°
Exp. critical inclination angle α 2D wave structure	−80.0°	−80.0°	−83.0°	−75.0°	−70.0°
Exp. critical inclination angle α 3D pyramid structure	−86.0°	−84.0°	−84.0°	−81.0°	−80.0°

Table 3 shows $\alpha_{critical}$ for different Reynolds numbers and the three investigated surface structures. The value for $\alpha_{critical}$ decreases with increasing Re, except for the outlier for Re = 37.88 and the 2D wave structure. This was verified by repeating the measurement once. Higher Reynolds numbers lead to higher film thickness (Fig. 7) and a wavier film flow, which is reinforced by the sharp edges of the 2D structure.

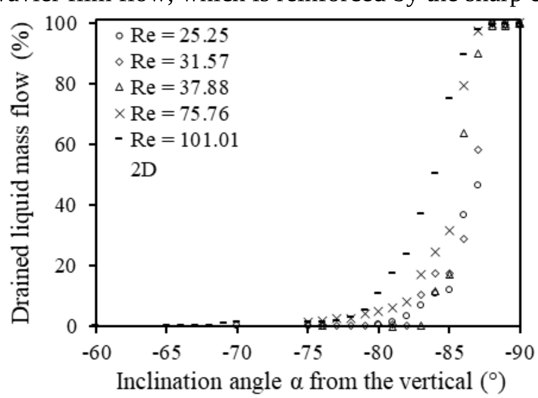

Fig. 5 Drained liquid mass flow for different Reynolds numbers over the inclination angle α (Ka = 1524, 2D).

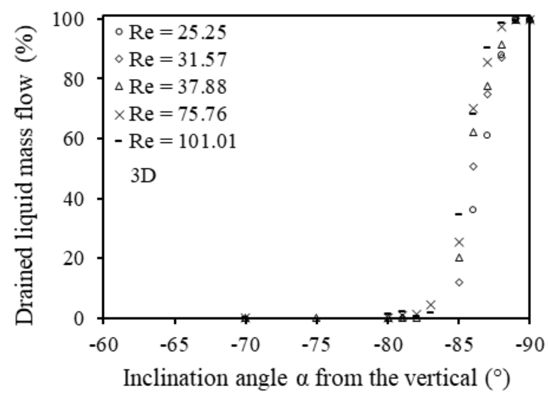

Fig. 6 Drained liquid mass flow for different Reynolds numbers over the inclination angle α (Ka = 1478, 3D).

In Fig. 5 and Fig. 6, the relative drained mass flow rates for the 2D wave structure and 3D pyramid structure are shown. For increased Reynolds number the relative drained mass flow increases as excepted for all structures. However, the dripping range of α is narrower for the 3D structure (Fig. 6) compared to the flat plate (Fig. 3) and the 2D structure (Fig. 5). This results in a similar draining behaviour for all Reynolds numbers for the 3D structure. The more negative $\alpha_{critical}$ and the similar draining behaviour for different Reynolds numbers show a profound stabilization effect of the 3D structure on the liquid film flow.

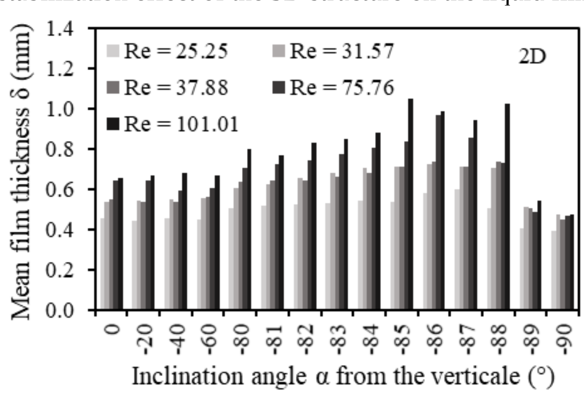

Fig. 7 Mean film thickness δ for 2D wave structure for different Reynolds number at 25°C with Ka = 1524.

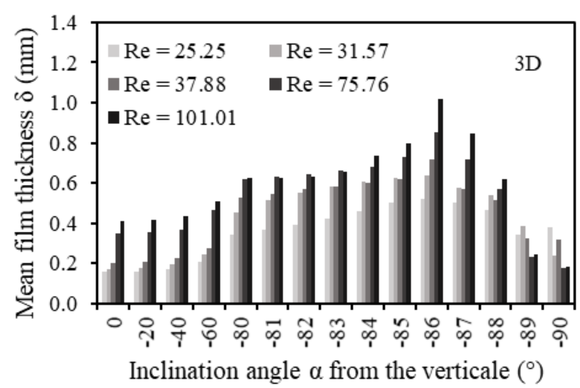

Fig. 8 Mean film thickness δ for 3D pyramid structure for different Reynolds number at 25°C with Ka = 1478.

Fig. 7 shows an increase of the mean film thickness with higher inclination for a 2D wave structure. Compared to the flat plate (Fig. 4) the mean film thickness is significantly higher, because the liquid flow must flow over the structure and so the liquid is accumulated. The overall increase of the film thickness is less pronounced than for the flat plate and almost no significant change in the range of α from 0° to −60° is observed. The film thickness for α from −89° to −90° results in a static hold up in the 2D structure. In Fig. 8, the mean film thickness for the 3D pyramid structure is shown for different Reynolds numbers. For Re from 25 to 38 and α from 0° to −60° the film thickness is smaller than the theoretical Nusselt film thickness. This might be due to acceleration of the fluid around the pyramid structure by means of continuity. Simultaneously, the cross-sectional area of the liquid flow does not increase proportionally, so that the overall mean film thickness appears smaller. For Re from 75 to 100 and α from 0° to −60° the mean film thickness is larger compared to the flat plate. The reason is still under numerical and experimental investigation and remains an open research question. Again, for α from −85° to −88° the measurement gets distorted by droplet detachment, whereas the static hold up can be observed for $\alpha \leq -89°$. In summary, a more even liquid distribution due to cross mixing induced by the 3D structure could be a reason for the stabilization of the liquid film flow.

Conclusion and outlook

Experimental results for measured critical inclination angle, relative drained mass flow, and mean film thickness of gravity-destabilized liquid films flows for different structured surfaces (flat, 2D wave, and 3D pyramid) are presented in this contribution. A good agreement between the simulation results from literature and experimental α and δ values was found. New experimental data for the two-dimensional and three-dimensional surface structure are shown, which intend to approximate real packing structures. For the 2D structure, a negative influence on the film flow stability was observed, which results in smaller absolute $\alpha_{critical}$ and a larger film thickness compared to the flat plate and the 3D pyramid structure. However, for the 3D structure we observed a stabilizing effect on the flow. In the future Kapitza numbers between 0.1 to 200, other Reynolds numbers and surface structures will be experimentally investigated to obtain experimental data for more viscous liquids. Overall, these results show the important influence of gravity-destabilized film flows in structured packings, which could be applied to the future design of high-performance packings for distillation and absorption.

Acknowledgements

Gefördert durch die Deutsche Forschungsgemeinschaft (DFG) – 426726119. Funded by the Deutsche Forschungs-gemeinschaft (DFG, German Research Foundation) – 426726119.

References

1. B. Scheid, N. Kofman and W. Rohlfs, *Physics of Fluids*, 28, 044107 (2016).
2. P.-T. Brun, A. Damiano, P. Rieu, G. Balestra and F. Gallaire, *Physics of Fluids*, 27, 084107 (2015).
3. A. Charogiannis, F. Denner, B.G.M. von Wachem, S. Kalliadasis, B. Scheid and C.N. Markides, *Physical Review Fluids*, 3, 114002 (2018).
4. N. Kofman, W. Rohlfs, F. Gallaire, B. Scheid, C. Ruyer-Quil, *International Journal of Multiphase Flow*, 104, (2018), 286-293.
5. P.L. Kapitza and S. Kapitza, *Zhurnal Eksperimentalnoi i Teoreticheskoi Fiziki* 19 (1949), 105-120.
6. H. Brauer, Bd. 2. Aarau und Frankfurt am Main: Sauerländer (1971), 674-685.
7. H. Brauer, VDI-*Forschungsheft* 457 (1956), VDI Verlag, Düsseldorf.
8. W. Nusselt, *Zeitschrift des Vereins deutscher Ingenieure* 60 (1916), 1645-1648.
9. L. Zhao and R. Cerro, *International journal of multiphase flow* 18.4 (1992), 495-516.
10. V. Bontozoglou and G.Pappolymerou, *International journal of multiphase flow* 23.1 (1997), 69-79.
11. M. Vlachogiannis and V. Bontozoglou, *Journal of Fluid Mechanics* 457 (2002), 133-156.
12. K. Argyriadi, M. Vlachogiannis and V. Bontozoglou, *Physics of Fluids* 18.1 (2006), 012102.
13. W. Rohlfs, P. Pischke and B. Scheid, *Physical Review Fluids* 2.4 (2017), 044003.